Journal of Solid State Chemistry **142,** 461–469 (1999)
Article ID jssc.1998.8068, available online at http://www.idealibrary.com on IDEAL®

Structure Determination and Physical Properties of the Misfit Layered Compound $(Pb_2FeS_3)_{0.58}NbS_2$

A. Lafond,*,[1] C. Deudon,* A. Meerschaut,* P. Palvadeau,* Y. Moëlo,* and A. Briggs†

*Laboratoire de Chimie des Solides, Institut des Matériaux de Nantes, UMR 6502 CNRS-Université de Nantes, 2, rue de la Houssinière, BP 32229, 44322 Nantes cedex 03, France; and †Centre de Recherche sur les Très Basses Tempèratures-CNRS 25, rue des Martyrs, BP 166X, 38042 Grenoble, France

Received June 29, 1998; in revised form October 5, 1998; accepted October 21, 1998

A crystal structure study of the layered misfit compound $(Pb_2FeS_3)_{0.58}NbS_2$ has been performed using the composite approach. The structure can be described on the basis of a regular alternation of $[Pb_2FeS_3]$ and $[NbS_2]$ slabs stacked along the *c* direction. The $[Pb_2FeS_3]$ part has a thickness of three layers, the central |FeS| layer being sandwiched between the two external |PbS| layers. Thus, Pb atoms on the exterior sides of this part are in a squared-pyramidal sulfur coordination, while Fe atoms in the central zone are octahedrally and tetrahedrally surrounded by sulfur atoms. From bond valence calculations, Fe atoms are found in the +III oxidation state whatever their environment. This is corroborated by a Mössbauer study. Magnetic and electrical properties complete this study. © 1999 Academic Press

Key Words: **sulfide; lead; iron; niobium; structure determination; Mössbauer; magnetism.**

INTRODUCTION

The study of misfit layer chalcogenides of chemical formulation $n(MX)_{1+x}\,m(TX_2)$ with M = Sn, Pb, Bi, Sb, rare-earth; T = Ti, V, Cr, Nb, Ta, Sn; X = S, Se; $1.08 < 1 + x < 1.28$; n = 1,2, and m = 1, 2, 3, … has aroused great interest in the structures, physical properties, and electronic energy band structures (1). In particular, the stability of these compounds has been widely debated, a partial answer being provided by the charge transfer (CT) mechanism. The importance of this point was demonstrated through $(LaS)_{1+x}CrS_2$, where the electron transfer from LaS (La^{3+} S^{2-} e^-) to CrS_2 is absolutely necessary for the existence of this phase (see Cario *et al.* (2)). Indeed, when transfer cannot take place as is the case for divalent cations ($M^{2+}X^{2-}$, e.g., M = Pb, Sn), the corresponding $(MX)_{1+x}CrX_2$ misfit compound does not exist.

Discussions concerning the oxidation state of metal atoms have been engaged around the question of charge transfer (3, 4). This consideration as well as the knowledge we have about homologous minerals has guided our research into the existence of new misfit material. So, in that way, Moëlo *et al.* (5) found a new derivative in the Pb/Fe/Nb/S system, belonging to the family of misfit compounds.

The building principle of such compounds consists of an alternating stacking sequence of two layered sets ($[MX] = Q$ and $[TX_2] = H$) giving a composite character to the structure.

Chronologically, the first reported synthetic misfit compound, $(LaS)_{1+x}CrS_2$, corresponded to the so-called monolayer type, in which the ratio n/m is equal to unity ($n = m = 1$). Here, the [LaS] part corresponds to the $[MX]$ pseudoquadratic layer ("Q"), and the $[CrS_2]$ part to the $[TX_2]$ pseudohexagonal one ("H"). Later on, mention of multilayer types was made through many examples of the bilayer type (6) (i.e., $n = 1$ and $m = 2$), and the trilayer type (7, 8) (i.e., $n = 1$ and $m = 3$). More recently, we synthesized a new misfit compound which illustrated the case for $n = 2$ and $m = 1$ (9), by derivation from the mineral franckeite (10). Now, with this new Pb/Fe/Nb/S compound, another type of homolog has been discovered. Indeed, the structure determination of this material $[1.5(Pb_{2/3}Fe_{1/3}S)_{1.16}NbS_2]$ $(\equiv(Pb_2FeS_3)_{0.58}NbS_2)$ shows that it corresponds to the type $n = 1.5$ for $m = 1$, which had never been observed before.

This paper deals with the preparation, crystal structure, magnetic, and transport properties and a room temperature Mössbauer study.

PREPARATION

Synthesis conditions have been reported in detail in a previous paper (5). A set of microanalyses with a Castaing electron microprobe has been performed on samples from the batch which gave the crystal selected for the structure

[1] To whom correspondence should be addressed. fax: (33) 2 40 37 39 95. E-mail: lafond@cnrs-imn.fr.

0022-4596/99 $30.00

study (Cameca Camebax system, for operating conditions, see (5)). The result is as follows (wt%, mean of 12 spot analyses, standard deviation in parentheses): Pb 50.50(43), Fe 5.47(11), Nb 20.26(32), S 24.69(15), sum = 100.92(67) wt%. On the basis of $\sum$cations = 2.74 at. $[(3 \times 0.58) + 1]$, the structural formula becomes $(Pb_{2.06}Fe_{0.83}Nb_{0.11}S_{3.05})_{0.58}NbS_2$. This formula is very close to that obtained initially; as pointed out previously (5), it may indicate that some Nb and Pb substitute for Fe, but more detailed data on various synthetic products (work in progress) can explain this deviation from the ideal formula as submicroscopic intergrowth with minor amounts of $1Q/1H$ homolog, $(PbS)_{1.14}NbS_2$.

STRUCTURAL DETERMINATION

A platelet-shape crystal with dimensions $0.11 \times 0.09 \times 0.01$ mm^3 was placed on an ENRAF-Nonius CAD4 diffractometer. Data collection was done into two separate stages reflecting the composite character of the compound:

— through the $h_1k_1l_1$ data set for the Q part ([(Pb/Fe)S]) whose unit cell parameters ($a_1 = 5.7632(7)$ Å, $b_1 = 5.7950(9)$ Å, $c_1 = 14.0805(12)$ Å) were determined from 25 reflections in the range $11.58^\circ < 2\theta < 43.8^\circ$;

— through the $h_2k_2l_2$ data set for the H part ([NbS_2]) whose unit cell parameters ($a_2 = 3.3279(3)$ Å, $b_2 = b_1$, $c_2 = c_1$) were refined from 25 reflections in the 2θ range 14.1°–43.8°.

Data collection conditions and crystallographic details are compiled in Table 1. All calculations were performed with the JANA chain programs (11). The structure determination was done in a composite approach, which means that each subpart (Q and H) was solved independently after reflections common to both subparts ($=0kl$) were excluded. However, these common reflections were used in a third step to find the relative arrangement (y and z coordinates) between Q and H entities.

TABLE 1
Data Collection Conditions and Refinement Results

Empirical formula	$(Pb_2FeS_3)_{0.58}NbS_2$
Crystal dimensions	$0.11 \times 0.09 \times 0.01$ mm^3 bounded by {100}, {010}, {001}
Absorption correction	Crystal shape; $\mu = 407$ cm^{-1}
Calculated density	$\rho = 5.93$ g cm^{-3}
Diffractometer	Enraf-Nonius CAD4
Radiation	Mo$K\alpha$ ($\lambda = 0.71069$ Å)
θ Range	$1.5^\circ \le \theta \le 38^\circ$
Scan mode	ω/θ, $\Delta\omega = 1.2 + 0.35 \tan\theta$
Indices range collection h, k, l	$-9, 9$; $-9,9$; 0, 25
Refinement results	
"Q" part	Formula: Pb_2FeS_3; $Z = 2$
Cell parameters (Å)	$a = 5.7632(7)$, $b = 5.7950(9)$, $c = 14.0805(12)$
Symmetry	Orthorhombic
Space group	*Cmmm*
Absorption correction T_{min}/T_{max}	0.045/0.663
No. of reflections $I \ge 3\sigma(I)$	324
No. of refined parameters	14
Reliability factors R*, R_w*	0.0486, 0.0348
Largest peaks in Fourier difference	$+3.7$ e$\cdot$Å^3; -4.9 e$^-\cdot$Å^3
"H" part	Formula: NbS_2; $Z = 2$
Cell parameters (Å)	$a = 3.3279(1)$, $b = 5.7950(9)$, $c = 14.0805(12)$
Symmetry	Orthorhombic
Space group	*Cm2m*
T_{min}/T_{max}	0.058/0.697
No. of reflections $I \ge 3\sigma(I)$	186
No. of refined parameters	7
Reliability factors R*, R_w*	0.0751, 0.0754
Largest peaks in Fourier difference	$+3.0$ e$^-\cdot$Å; -2.8 e$^-\cdot$Å^3
Common part	
Space group	*Cm2m*
No. of reflections $I \ge 2.5\sigma(I)$	82
No. of refined parameters	8
Reliability factors R*, R_w*	0.0889, 0.0967

Note. $*R = \sum(|F_{obs}| - |F_{calc}|)/\sum(F_{obs})$;
$R_w = (\sum w(|F_{obs}| - |F_{calc}|)^2/\sum w(F_{obs})^2)^{1/2}$; $w = 1$.

1. *Refinement of the* [(*Pb*, *Fe*)*S*] *Part* (*Q Part*)

As a result of a preliminary X-ray study on a Weissenberg camera, the C-centering condition ($h + k = 2n$) was initially applied as a data recording condition for the CAD4 diffractometer. No other systematic existing condition was imposed.

The Pb position was found via a Patterson map; the remaining positions for Fe and S atoms were deduced from subsequent difference-Fourier syntheses. Thus, in the course of this structure determination done in the space group (SG) *Cmmm* (No. 65), it appeared that the Fe positions had to be split into five groups, i.e., a central one at 1/2,0,0 (site 2b), and four symmetrical others on the 8(p)-site (x,y,0; $-x$, $-y$,0; $-x$,y,0; x, $-y$,0) with $x \approx 0.41$ and $y \approx 0.09$ (see Figs. 1 and 3). Sulfur atoms coordinated to these Fe atoms were also statistically distributed over a four-site disorder corresponding to the 8(p) site with $x \approx 0.96$ and $y \approx 0.04$. Occupancy factors for all these split positions (Fe and S sites) were constrained such that their summation corresponded to a total occupation of the nonsplit central positions (i.e., $\frac{1}{2}$ 0 0 and 0 0 0, respectively). Refinements performed on data noncorrected for absorption effects converged to reliability factors of $R = 9.67\%$ and $R_w = 7.91\%$ for 326 unique reflections with $I > 3\sigma(I)$ and 14 variables, Pb atoms being refined anisotropically. A difference-Fourier calculation done after this refinement showed that the two largest residual peaks were located on either side of the Pb atom at $\Delta z \approx \pm 0.05$ along the **c** direction; this meant a much too close contact (< 1 Å) with the initial central Pb atom.

Absorption corrections based on the dimensions of the crystal were then applied. It resulted in much lower

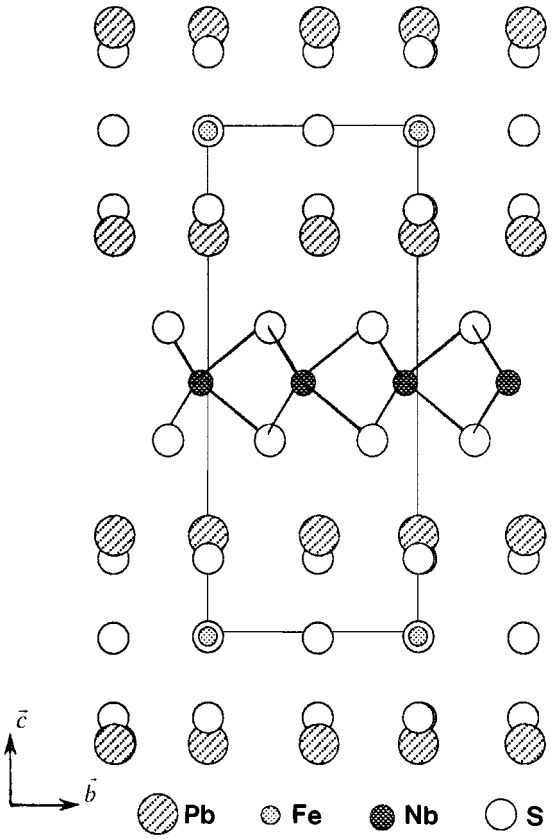

FIG. 1. Projection of the whole structure of $(Pb_2FeS_3)_{0.58}NbS_2$ onto the (*b*,*c*) plane. In order to make the figure more readable only the central positions of the iron atoms (0,0,0) and sulfur atoms (0.5,0,0) have been drawn.

reliability factors $R = 4.86\%$ and $R_w = 3.48\%$ for 324 reflections with 14 variables, i.e., taking into account the same constraints as discussed above. This time the final difference-Fourier map showed no significant residuals.

A refinement in the noncentrosymmetric space group *Cm*2*m* (No. 38) was tried concerning the Fe-split positions along the *a* and/or *b* direction. Thus, as only Fe and associated S atoms were concerned with a statistical occupancy corresponding to y and $-y$ coordinates (mirror plane perpendicular to the *b* axis), refinement with similar constraints as discussed above, conducted in the space group *Cm*2*m*, implied here a choice for Fe/S sites, i.e., either at $+y$ or at $-y$ values. In fact, all the y coordinates for any atoms (except only one which needs to be fixed for origin) were free to vary. No improvement in the resulting reliability factors was observed for this attempt.

The possible substitution of Fe by Nb or Pb, especially on the Fe1 position, was tentatively explored but without any success, which confirms the interpretation of electron probe microanalysis.

Thus, the final choice for the space group was *Cmmm*. Final values of atomic coordinates and isotropic/anisotropic thermal parameters obtained from a refinement of corrected intensities (absorption effects) are given in Tables 2 and 3, respectively. The rather large negative residual peak in the Fourier difference synthesis (-4.9 e$^-$ Å^{-3}), localized near the Pb site, is certainly due to the displacive modulation of atoms lying on the outer sides of the *Q*-layer (Pb and S1) which are more sensitive to the presence of the adjacent *H*-layers.

TABLE 2
Atomic Coordinates for the "*Q*" part (SG *Cmmm*, No. 65)

Atom	Site	SOF[a]	x	y	z	U_{eq}(*) or U_{iso}
Pb	4k	1	0	0	0.20530(7)	*0.0221(2)
S1	4l	1	1/2	0	0.1555(4)	0.0203(9)
Fe1	2b	0.2491(11)	1/2	0	0	0.019(2)
Fe2	8p	0.1878(–)	0.4107(13)	0.085(2)	0	0.019(–)
S2	8p	1/4	0.9600(14)	0.041(2)	0	0.012(3)

Note. [a] SOF, site occupancy factor.

2. *Refinement of the NbS_2 Part (H Part)*

The C-centering condition was also imposed in the CAD4 data recording conditions. The Nb and S positions were deduced from a Patterson map analysis. Refinements, which were conducted in the noncentrosymmetric space group *Cm*2*m*, led to reliability factors of $R = 8.31\%$ and $R_w = 9.03\%$ for 186 unique reflections, noncorrected for absorption, satisfying $I > 3\sigma(I)$ with seven variables. Under the same conditions, refinement of corrected intensities gave a better result, i.e., $R = 7.51\%$ and $R_w = 7.54\%$. A final difference-Fourier calculation was featureless. Table 4 summarizes atomic and isotropic thermal parameters and Table 3 the anisotropic thermal parameters for Nb atoms.

3. *Refinement of the Common Part*

The relative origin of the two sublattices (*Q* and *H*) was obtained from the refinement of the 0*kl* reflections which are common to both parts. These reflections were corrected for absorption effects. Refinements were performed in the space group *Cm*2*m*. The starting point was the y and z coordinates of all the atoms obtained in the earlier refinements. The

TABLE 3
Anisotropic Temperature Parameters for Pb and Nb Atoms

Atom	U_{11}	U_{22}	U_{33}	U_{12}	U_{13}	U_{23}
Pb	0.0311(3)	0.0222(3)	0.0131(3)	0	0	0
Nb	0.0114(9)	0.0034(9)	0.0015(11)	0	0	0

TABLE 4
Atomic Coordinates for the "*H*" Part (SG *Cm2m*, No. 38)

Atom	Site	SOF[a]	x	y	z	U_{eq} (*) or U_{iso}
Nb	2b	1	0	0	1/2	*0.0054 (5)
S3	4c	1	0	0.3332(9)	0.3884(4)	0.0113(12)

Note. [a] SOF, site occupancy factor.

z coordinates of all the atoms were left unchanged as were the y coordinates of the atoms of the Q-part. All the y coordinates of atoms in the H-part were changed by the same Δy which was used as an optimisation parameter for the 0kl reflections. The relative diffracting weight between Q and H subparts was fixed in agreement with the mismatch ratio $a_H/a_Q = 0.58$ which normalizes the contribution of each part to the same volume. The final refinement converged to reliability factors $R = 8.89\%$ and $R_w = 9.67\%$ for 82 reflections satisfying $I > 2.5\sigma(I)$, with eight variables. Atomic coordinates and isotropic thermal parameters are reported in Table 5.

DESCRIPTION OF THE STRUCTURE

Figure 1 shows the projection of the whole structure of $(Pb_2FeS_3)_{0.58}NbS_2$ onto the (b,c) plane as deduced from refinement of the common part.

The Q-part defined as the $[Pb_2FeS_3]$ slab is built up from three [MS] layers (M = Pb, Fe) stacked along the c direction, the two external layers being [PbS] which enclose the [FeS] layer. Coordination types of the metal atoms are either squared-pyramidal for Pb atoms or pseudooctahedral for the Fe atoms. The five closest S neighbors around Pb atoms, S atoms within this slab, are at an average distance of 2.971 Å; the apical Pb–S distance (2.908 Å) is shorter than the four planar ones relative to the square arrangement of S atoms (see Fig. 2a). In addition, Pb atoms which protrude from the S plane are also coordinated with one or two S atoms belonging to the NbS_2 slab. Because of incommensurability, this number cannot be defined; i.e., these Pb–S interslab distances vary between lower and upper limits with respect to the difference between a_1 and a_2 unit cell parameters.

Fe atoms located in the central zone of the Q-part are surrounded by S atoms roughly distributed over an octahedral polyhedron (Fig. 2b). This means that the special position (2b) for the central Fe1 atom corresponds to a slightly distorted octahedral coordination whereas the split Fe2 positions (on four sites) are rather indicative of a distorted tetrahedral coordination around these atoms (see Fig. 2b). Table 6 gathers together all the possible interatomic M–S distances (there will be a choice between them because of a statistical occupancy) around each type of polyhedron and the bond valence values calculated with these M–S distances, using the bond valence parameters R_{ij} tabulated by Brese and O'Keeffe (12). It thus appears that Fe atoms are in the +III state. The situation of the Fe atoms has to be given in detail because of the split positions of both the Fe and their closest S atoms. Thus the central Fe1 atom is surrounded by S2 atoms statistically occupying eight positions (four groups of two, which groups are identical two by two because of centrosymmetry) in the (a, b) plane (see Fig. 3). This results in two very slightly different distances (2.661 and 2.668 Å) and a bond valence sum of 2.88. If we consider the Fe2 atom in its tetrahedral coordination (see Fig. 2b), once again each S2 position corresponds to four split sites. In Table 6, only the four shortest Fe–S2 distances are reported (two in a direction parallel to a, the two others in a direction parallel to b). This implies a choice of two S2 atoms among the four mentioned. Taking into account the two shortest Fe–S2 distances, the summation of bond valence gives 3.33, whereas the two longest Fe–S2 distances would lead to 2.84. Whatever the choice, the +III oxidation state for all Fe atoms seems to be ascertained. This feature will be discussed below.

The H-slab is very similar to that found in the parent misfit compound $(MX)_{1+x}NbS_2$ as well as in the pure binary NbS_2 itself, which means Nb atoms are within a trigonal prism of S atoms (Fig. 2c). The Nb–S distances are quasi-identical with those commonly encountered (see Table 6).

TABLE 5
Atomic Coordinates for the Common Part (SG *Cm2m*: No. 38)

Atom	Site	SOF[a]	x	y	z	U_{iso}
Pb	4c	0.5774(–)	—	0	0.20530(–)	0.0205(10)
S1	4c	0.5774(–)	—	0	0.1555(–)	0.061(11)
Fe1	2a	0.1436(–)	—	0	0	0.003(7)
Fe21	4d	0.1084(–)	—	0.085	0	0.003(–)
Fe22	4d	0.1084(–)	—	−0.085	0	0.003(–)
S21	4d	0.1444(–)	—	0.041	0	0.016(14)
S22	4d	0.1444(–)	—	−0.041	0	0.016(–)
Nb	2b	1	—	−0.0681(12)	1/2	0.0051(12)
S3	4c	1	—	0.2651(12)	0.3884	0.011(2)

Note. [a] SOF, site occupancy factor.

RESISTIVITY MEASUREMENTS

Resistance measurements were performed with a precision a.c. bridge using a four-probe method (van der Pauw configuration) in the temperature range 0.35–290 K. The uncertainty in estimating the thickness (about 6 μm) is very large; then, the error in the resistivity is about 50%. Figure 4 shows the thermal dependence of the resistivity in the temperature range 4.2–290 K. The Pb/Fe/Nb/S compound has

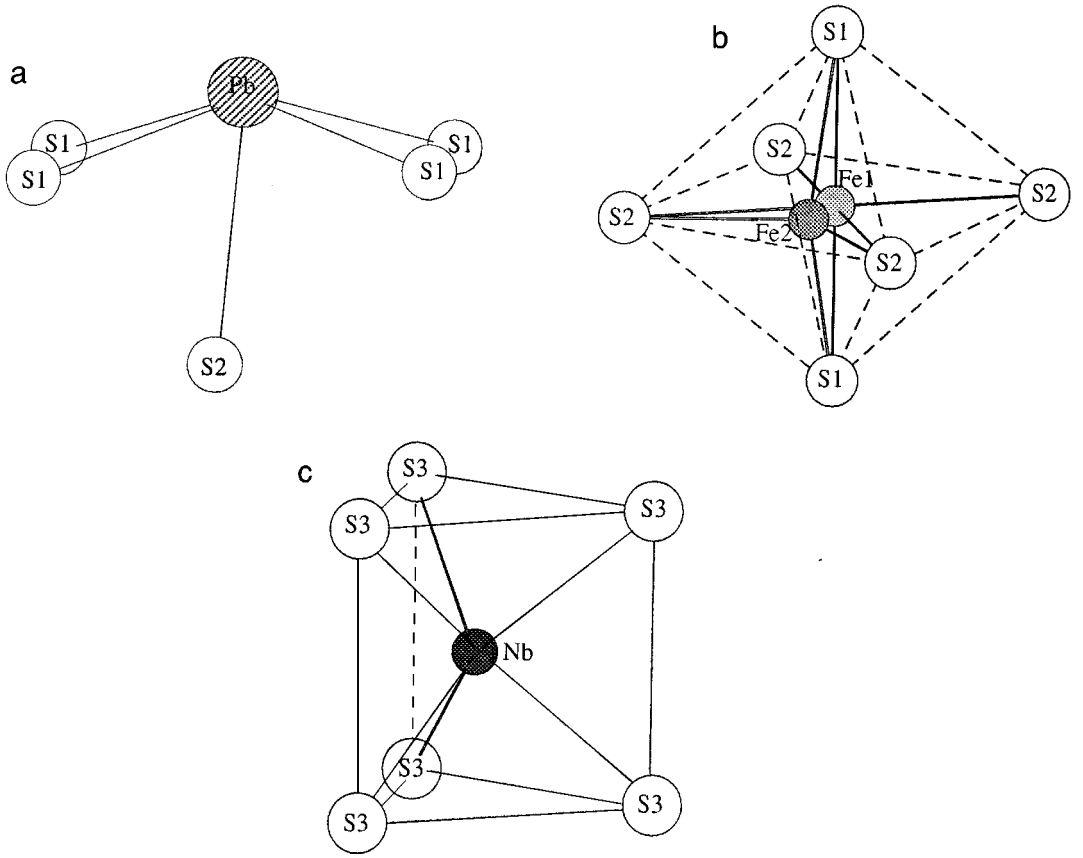

FIG. 2. Cationic environments in $(Pb_2FeS_3)_{0.58}NbS_2$ (for clarity, only one S2 or/and one Fe2 position among the four possible ones is indicated). (a) Environment of Pb atoms; (b) transformation from octahedral coordination (around Fe1) to a tetrahedral one (around Fe2); (c) environment of Nb atoms

a metallic behavior without any superconducting transition down to 350 mK. Although the compound is expected to be very anisotropic, measurements of the perpendicular conductivity were not attempted because we have not yet developed a reliable method. The four terminal technique is difficult on small specimens; and a simple two wire method gives, because of contact resistances, false values for the anisotropy.

TABLE 6
Set of Interactomic Distances

Atom 1	Atom 2	SO[a]	Valence	Distance (Å)	Atom 1	Atom 2	SO[a]	Valence	Distance (Å)
Pb	$2\times$S1	#0, #9		2.9649 (12)	Fe2	$2\times$S1	#0, #1	0.68	2.302 (6)
	$2\times$S1	#6, #8		2.9762 (12)		S2	#2	1.02	2.152 (11)
	$1\times$S2	#1, #2,		2.9080 (14)		S2	#7	0.94	2.182 (16)
		#9, #10				S2	#1	0.77	2.257(12
						S2	#4	0.71	2.288 (15)
Fe1	$2\times$S1	#0, #1	0.93	2.189 (5)					
	$2\times$S2	#0, #1	0.26	2.661 (8)		S2		0.30	2.610 (11)
		#2, #3							
	$2\times$S2	#6, #7	0.25	2.668(11)		S2		0.27	2.648 (16)
		#4, #5							
			$\sum \approx 2.88$					$\sum \approx 2.84 - 3.32$	
Nb	$4\times$S3			2.482 (4)					
	$2\times$S3			2.483 (5)					

[a] SO, symmetry operations: #1 $1-x, -y, -z$; #2 $1-x, y, z$; #3 $x, -y, -z$; #4 $3/2-x, 1/2-y, -z$; #5 $3/2-x, -1/2+y, z$; #6 $-1/2+x, -1/2+y, z$ #7 $-1/2+x, 1/2-y, -z$; #8 $-1/2+x, 1/2+y, z$; #9 $-1+x, y, z$; #10 $-1+x, -y, -z$.

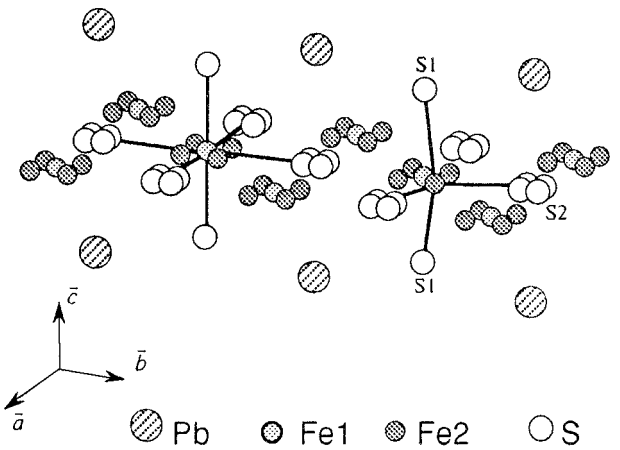

FIG. 3. View of the splitting of Fe and S atoms in the Q part of $(Pb_2FeS_3)_{0.58}NbS_2$. Octahedral and tetrahedral environments of iron atoms are shown.

MAGNETIC MEASUREMENTS

Magnetic measurements have been performed with the use of a SQUID magnetometer working between 2 and 300 K in the field range 0–5 T. These measurements have been made on a powder sample ($m \approx 200$ mg). Thermal dependence of the susceptibility (M/H) was studied for two different cooling modes. The sample was introduced in the magnetometer at a "high" temperature (paramagnetic domain) and cooled in zero field (ZFC) down to the starting temperature. ZFC data were then collected during the warming process after applying the field. In a second step, the sample was cooled under this applied field (FC) and measurements were again taken with increasing temperature. Raw data were corrected for the contribution of the sample holder ($\approx 1\%$). Then the diamagnetism of the core electrons (-4.5×10^{-4} emu mol^{-1}) was substracted from the ratio M/H to get the magnetic susceptibility per formula unit deduced from the microprobe analysis ($Pb_{2.48}FeNb_{2.23}S_{7.83}$).

Figure 5 shows the thermal dependence of the ZFC and FC susceptibilities for two values of the applied field and the inverse susceptibility versus T in the high temperature range. One can see a field-dependent hysteresis between ZFC and FC data below 25 K. The difference between these curves can be explained by the freezing of the magnetic moments in a disordered state during the ZFC process. This behavior is reminiscent of that of the misfit compound $(La_{0.95}[\ ]_{0.05}S)_{1.19}CrS_2$ (13), where it could be related to the incommensurate character of the structure which led to a large distribution of interactions between the magnetic atoms. The plot of $1/\chi$ versus T (Fig. 5) indicates that the paramagnetic behavior of this phase is also complex. The downward curvature is not consistent with a simple Curie–Weiss law. Attempts to fit these high temperature data by including a thermally independent paramagnetism (T.I.P.) term χ_o ($\chi = C/(T-\theta) + \chi_o$) led to $C = 0.80(1)$ emu·K/(mol·Fe), $\theta = -13(1)$ K, and $\chi_o = 2.6(1) \times 10^{-3}$ emu/(mol·Fe) (see the susceptibility curve fit on Fig. 5). Figure 6 shows the contribution of the localized electrons ($\chi - \chi_o$). The very small value of the Curie constant

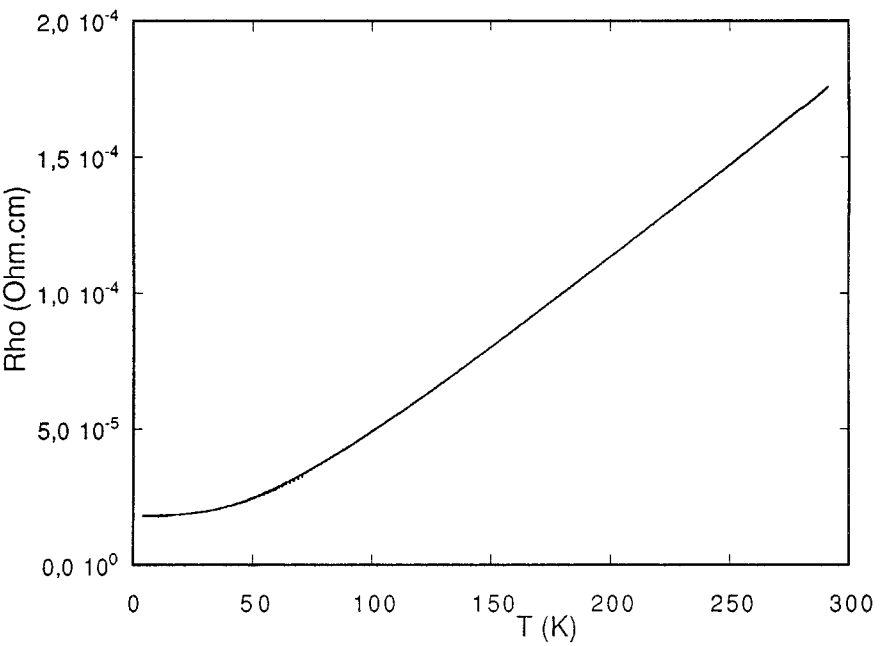

FIG. 4. Variation of the resistivity (parallel to the layers) of $(Pb_2FeS_3)_{0.58}NbS_2$ versus temperature assuming a thickness of the crystal about 6 μm.

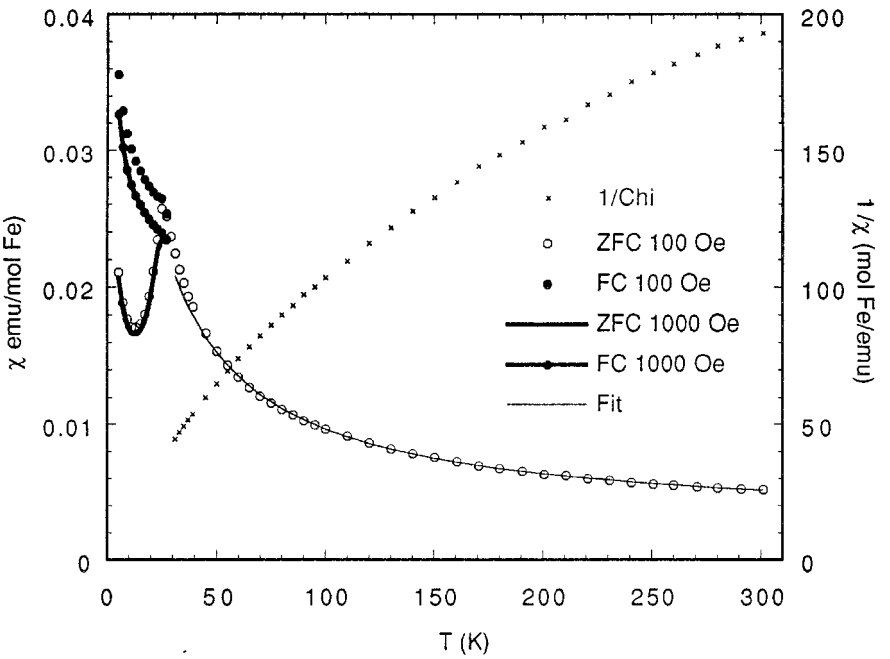

FIG. 5. Thermal dependence of the *d–c* magnetic susceptibility of $(Pb_2FeS_3)_{0.58}NbS_2$ for two cooling modes and for two magnetic field strengths. Above 30 K, only ZFC data for $H = 100$ Oe have been drawn. The high temperature-range line is the fitted curve according to the model: $\chi = C/(T - \theta) + \chi_o$ (see text).

disagrees totally with the fully localized, high spin magnetism of Fe^{2+} ($C = 3.0$ emu·K mol^{-1}) or Fe^{3+} ($C = 4.4$ emu·K mol^{-1}). Possible occurrence of a spin state mixture (low spin–high spin) will be discussed hereafter. The value of the T.I.P. parameter is of the same order of magnitude as in some other Fe/Nb chalcogenides such as $Fe_{1+x}Nb_{3-x}Se_{10}$ ($0.25 < x < 0.40$) (14, 15). The large value of χ_o can be correlated to the metallic character of this compound with

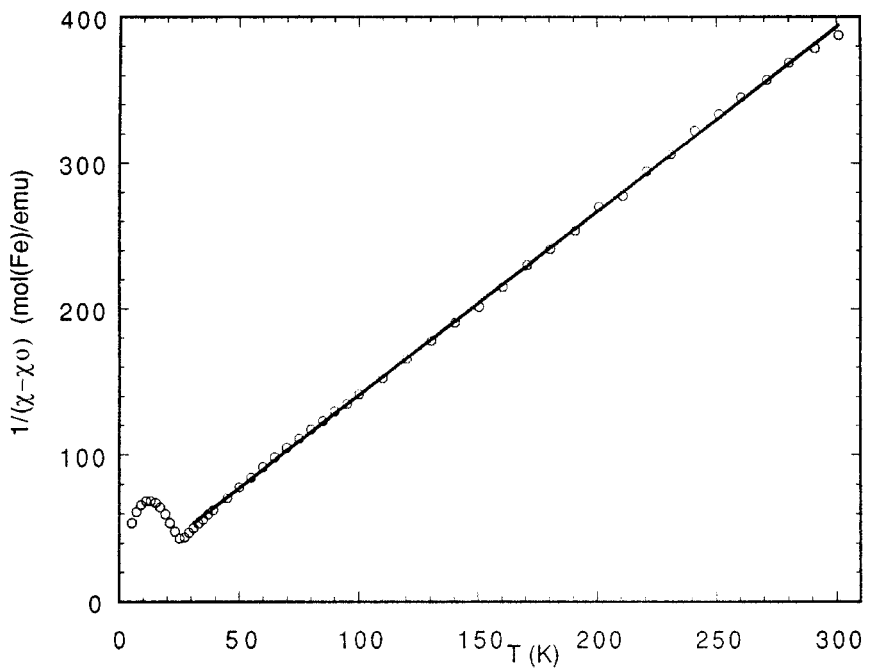

FIG. 6. The thermal variation of inverse ZFC susceptibility corrected by the TIP contribution of $(Pb_2FeS_3)_{0.58}NbS_2$.

exchange Stoner-enhancement: $\chi_o = \chi_p/(1 - U \times N(E_F))$, where $N(E_F)$ is the density of states at the Fermi level, U the interaction between electrons, and χ_p the Pauli paramagnetism ($\chi_p = 2N_A\mu_B^2 N(E_F)$). It is known that the T.I.P. parameter is larger in *d*-compounds than s or p ones due to a large value of $U \times N(E_F)$ (i.e., close to 1).

MÖSSBAUER SPECTROSCOPY

Mössbauer spectra were obtained with a constant acceleration automatic folding Elscint type spectrometer using a room temperature ^{57}Co source in a transmission geometry. Fe_α was used as a standard reference. Spectra were computed with a least squares routine using Lorentzian lines. Spectra recording was complicated by the small amount of iron in the structure (wt % $\approx$ 5) and the presence of a heavy absorbing element (Pb). Indeed, a long acquisition time, at least 2 weeks, was necessary to obtain a reliable spectrum. For this reason measurements for obtaining the temperature dependence of the Mössbauer behavior were not undertaken, even though such a study would be very interesting to determine a possible high spin–low spin transition.

The resulting spectrum (Fig. 7) is nonsymmetric and the best fit is obtained with the superposition of three quadrupole doublets whose intensity ratios are roughly 2-1-1 (Table 7).

Isomer shift values (δ) are lower than those observed in $Fe_{1+x}Nb_{3-x}Se_{10}$ (0.50 mm s^{-1}; 0.46 mm s^{-1} (14, 15),

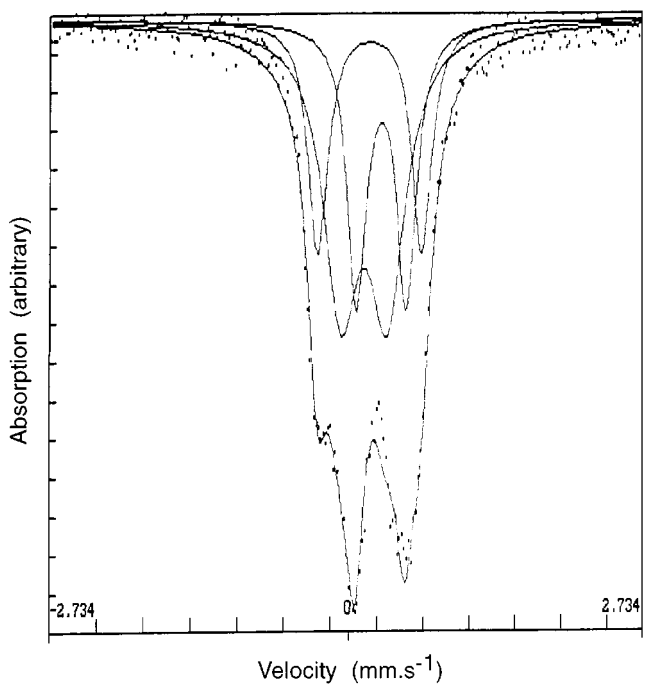

FIG. 7. ^{57}Fe Mössbauer spectrum of $(Pb_2FeS_3)_{0.58}NbS_2$; lines correspond to the fit with three different sites for Fe atoms. Dots represent experimental spectrum.

TABLE 7
Mössbauer Parameters (mm s^{-1}) at 300 K

Site	δ	ΔE	w	%
1	0.41	0.46	0.11	28
2	0.25	0.43	0.20	48
3	0.30	0.96	0.11	24

Note. δ Isomer shift (Fe α as reference); ΔE, quadrupole splitting = $1/2\ eV_{zz}Q(1 + \eta^{2/3})^{1/2}$; w, half linewidth at half height.

respectively) in which iron was found to be in an octahedral environment. They are similar to those observed in amorphous Fe_2S_3 (0.23–0.39 mm s^{-1}) (16). In this sulfide compound, two types of iron are located on two different symmetry sites, tetrahedral, and octahedral.

DISCUSSION

In the heart of the Q part, the (Fe, S) plane shows multiple-split sites for both Fe and S atoms. Thus, Fe atoms are statistically shared between five very close sites, i.e., a central one and four equivalent symmetrical ones, whereas S atoms are distributed over four close sites.

Under these conditions, it is not easy to determine which distribution of occupied sites really exists. The Mössbauer spectroscopy which acts as a local probe should indicate what kind of Fe polyhedra are the most probable and give a good estimation of the mean oxidation state of iron atoms.

The δ value of the site 1 (0.41 mm s^{-1}) is in agreement with isomer shifts observed in the case of iron Fe(III) in octahedral sulfur environments. This site can be associated with the Fe1 crystallographic site identified from the structural determination which is located at the center of an octahedron. The quadrupole splitting $\Delta E = 0.46$ mm s^{-1} corresponds to an axial distortion of the octahedron due to different distances between iron and sulfur atoms. Iron (Fe1) is surrounded by four sulfur atoms (S2) in the same plane at 2.66 Å and two apical sulfur atoms (S1) at a shorter distance: 2.19 Å (Fig. 2b). This site represents 28% of the total absorption, in agreement with crystallographic results, Fe1 being in position 2b and Fe2 in position 8p.

Isomer shift values on sites 2 and 3 are lower and very close to those observed in Fe_2S_3 for Fe(III) in a tetrahedral symmetry. If we consider the structural results, Fe2 is indeed in a tetrahedral coordination. However, this iron is randomly distributed over four positions (Fig. 3). The first neighbors are four sulfur atoms at a mean distance of $\approx$2.2 Å in a distorted tetrahedral environment. As expected the metal-sulfur distances are significantly shorter than in an octahedral coordination. However, we must also keep in mind that sulfur atoms are distributed on four statistical positions, giving other longer iron–sulfur distances (2.70 Å). These different near-neighbor distributions may explain why in

Mössbauer spectroscopy this site is split in two with very different quadrupole splitting (0.43 and 0.96 mm s^{-1}) and similar isomer shifts (0.25–0.30 mm s^{-1}). The broadening of the lines, particularly evident for the site 3 is assumed to arise from the simultaneous cation and anion randomness. Another consequence of the cation distribution is that the shortest possible Fe–Fe distance (2.65 Å) is significantly shorter than the Goodenough critical value (≈ 3 Å) for metal–metal direct interactions. Such interactions can induce a delocalization of the 3*d* electrons expected in a metallic conductor and thus increase the complexity of the Mössbauer spectra.

It is clear that it is impossible to assign one doublet to a tetrahedron with short Fe–S distances and the other to long Fe–S distances. Probably the two doublets correspond to a mean distribution. The higher ΔE value for site 3 can be partially due to direct iron-iron interactions which may also slightly increase the isomer shift. The environment of iron in this site would be in fact, based not only on four sulfur atoms but on four sulfur atoms and one iron. The probability of having this situation is low and explains why the intensity of this site is only one half of the other one.

A valence state estimation based on relations between isomer shifts and oxidation states in sulfur environments, established by Fatseas and Goodenough (17) leads to a formal valency of 2.88 for Fe1 in octahedral coordination, and 2.86 and 2.65, respectively for the two Fe2 tetrahedral sites. These values agree well with bond valence calculations (Table 6)

The very low value of the Curie constant deduced from magnetic measurements could be explained by the presence of iron in low spin state. This configuration is well known in iron sulfides (18, 19). Our Mössbauer data could be consistent with the possibility of such a spin state as observed in $Tl_{0.95}V_4FeS_8$ (20). However, the crystallographic environment of iron atoms in this structure is so complex that it is impossible to give a more precise explanation of magnetic and Mössbauer results.

CONCLUSION

The crystal structure of $(Pb_2FeS_3)_{0.58}NbS_2$ corresponds to a new type of homolog in the family of layered misfit chalcogenides. It reveals an unusual complexity of the *Q* layer, due to the coexistence of two coordinations for Fe. Such a complexity is absent in the very comparable structure exhibited by $(Eu_3S_3)_{0.575}NbS_2$, very recently reported as $[(EuS)_{1.5}]_{1.15}NbS_2$ (21). Indeed, Eu1 and S1 atoms located in the central layer within the *Q* part are on special positions instead of split ones for the (Pb,Fe) derivative. This structural difference is likely associated with a size effect, $r(Eu^{3+})$ being larger than $r(Fe^{3+})$. The mixed valence state for Eu atoms viz. +III for Eu1 atoms and +II for Eu2 atoms (on the outer sides of the *Q* layer) was established from a bond valence calculation. This result, incidentally, reinforces our assumption about the Fe(III) state in the $(Pb_2FeS_3)_{0.58}NbS_2$ compound.

Another originality of this compound is the combination of magnetic properties due to trivalent Fe in the *Q* layer with metallic character due to the H layer. Nevertheless, the charge transfer from *Q* to *H* layer is very high (0.58 e^-, corresponding to a formal valence of 3.42 for Nb); this would explain the absence of superconductivity according to the model proposed by Moëlo *et al.* (22).

As pointed out in the crystal chemical discussion about this compound (5), other compounds belonging to this homologous type may be envisaged with other cations, or replacing S by Se. Such new syntheses are in progress, in order to help to explain the physical properties of this first compound and to search for new phases combining magnetic properties and superconductivity.

REFERENCES

1. G. A. Wiegers and A. Meerschaut, *Mater. Sci. Forum* **100&101,** 101 (1992).
2. L. Cario, D. Johrendt, A. Lafond, C. Felser, A. Meerschaut, and J. Rouxel, *Phys. Rev. B* **55,** 9409 (1997).
3. Y. Ohno, *Solid State Commun.* **79,** 1081 (1991).
4. A. R. H. F. Ettema and C. Haas, *J. Phys. Condens. Matter* **5**, 3817 (1993).
5. Y. Moëlo, A. lafond, C. Deudon, N. Coulon, M. Lancin, and A. Meerschaut, *C.R. Acad. Sci.* **325,** 287 (1997).
6. A. Meerschaut, L. Guemas, C. Auriel, and J. Rouxel, *Eur. J. Solid State Inorg. Chem.* **27,** 557 (1990).
7. Y. Oosawa, Y. Gotoh, J. Akimoto, T. Tsunoda, M. Sohma, and M. Onada, *Jpn. J. Appl. Phys.* **31,** 1096 (1992)
8. L. M. Hoistad, A. Meerschaut, P. Bonneau, and J. Rouxel, *J. Solid State Chem*, **114,** 435 (1995).
9. A. Lafond, A. Meerschaut, Y. Moëlo, J. Rouxel, *C.R. Acad. Sci. Paris* **322,** 165 (1996).
10. Y. Moëlo, E. Mackovicky, B. Karup Møller, and C. Maurel, *Eur. J. Miner.* **2,** 711 (1990).
11. V. Petricek and M. Dušek, JANA 96 Crystallographic computing System.
12. N. E. Brese and M. O'Keeffe, *Acta Crystallogr. B* **47,** 192 (1991).
13. A. Lafond, A. Meerschaut, J. L. Tholence, A. Sulpice, and J. Rouxel, *Phys. Rev. B* **52,** 1112 (1995)
14. A. Ben Salem, G. Fatseas, P. Molinie, and A. Meerschaut, *Synth. Met.* **25,** 207 (1988).
15. R. J. Cava, F. J. Di Salvo, M Eibschutz, and J. V. Waszczak, *Phys. Rev. B* **27**, 7412 (1983).
16. A. H. Stiller, B. J. McCormick, P. Russel, and P. A. Montano, *J. Am. Chem. Soc.* **100,** 2554 (1978).
17. J. B. Goodenough and G. A. Fatseas, *J. Solid State Chem.* **41,** 1 (1982).
18. C. A. McCammon and D. C. Price, *J. Phys. Chem. Solids* **43**(5), 431 (1982).
19. F. J. DiSalvo, M. Eibschutz, C. Cros, D. W. Murphy, and J. V. Waszczak, *Phys. Rev. B* **19**(7), 3441 (1979).
20. W. Bensch, R. Schlögl, and E. Amberger, *Helvetica Chemica Acta* **69,** 35 (1986).
21. L. Cario, A. Meerschaut, C. Deudon, and J. Rouxel, *C.R. Acad. Sci. Paris* **1,** (IIc), 269 (1998).
22. Y. Moëlo, A. Meerschaut, J. Rouxel, and C. Auriel, *Chem. Mater.* **7,** 1759 (1995).